Supporting information

Boosting Thermoelectric Performance of Calcium Cobaltite Composites Through Structural Defect Engineering

Zongmo Shi[1,4], Can Zhang[1], Taichao Su[2], Jie Xu[1,4], Jihong Zhu[3,4], Haiyan Chen[1], Tong Gao[3,4], Mengjie Qin[1,4], Ping Zhang[1,4], Yi Zhang[1,4], Haixue Yan[4,5], and Feng Gao[1,4*]

1 State Key Laboratory of Solidification Processing, MIIT Key laboratory of Radiation Detection Materials and Devices, USI Institute of Intelligence Materials and Structure, School of Material Science and Engineering, Northwestern Polytechnical University, Xi'an, 710072, P. R. China

2 School of Materials Science and Engineering, Henan Polytechnic University, Jiaozuo, 454003, P. R. China

3 State IJR Center of Aerospace Design and Additive Manufacturing, MIIT Lab of Metal Additive Manufacturing and Innovative Design, Northwestern Polytechnical University, Xi'an, 710072, P. R. China

4 NPU-QMUL Joint Research Institute of Advanced Materials and Structure, Northwestern Polytechnical University, Xi'an, 710072, P. R. China

5 School of Engineering and Materials Science, Queen Mary University of London, London, E1 4NS, United Kingdom

[*] Corresponding author:

F. Gao, E-mail address: gaofeng@nwpu.edu.cn

Figure S1 shows the XPS spectra of the composites accounted for the structural defects. The peaks of La 3*d*, Co 2*p*, Co 3*s*, Co 3*p*, Ag 3*p*, Ag 3*d*, Ca 2*s*, Ca 2*p*, O 1*s*, and O KLL were observed in the full survey spectra, indicating that Ag^{+} and La^{3+} were successfully introduced into the crystal lattice [S1], corresponding well to the EDX mappings. Two doublets Ag 3*d* peaks were fitted and distinguished, as shown in Figure S1 (b). Ag 3*d* peaks were detected with the banding energy of 368.0 eV and 365.7 eV to identify the incorporation of metallic Ag and lattice Ag^{+}. The specific ratios of sliver were calculated and shown in **Table** S1.

Figure S2 shows the XPS fitting results about O element. The peaks at 531.3 eV was associated with Co-O bonds and Ca-O bonds, implying the lattice oxygen on its intrinsic sites. It presented as well the peaks located at 533.1 eV and 534.0 eV for oxygen vacancy and chemical absorbed oxygen on the surface, respectively [S2].

Figure S3 show two spin-orbital doublets of Co 2*p* and the spin-state transition scenario, which could be distinguished by the XPS fitting results. The spin entropy of Co^{3+} and Co^{4+} was suggested to account for the formation of the three mentioned oxygen [S3]. Due to compensate mechanism of charge carrier, there was considerable interest in the reduction of lattice Ag^{+} accompanying with increasing of La^{3+} dopant levels. The Co 2*p* peaks presents the two distinct peaks and located at 799.4 eV and 781.0 eV, respectively, which matched well to the Co^{3+} and Co^{4+}. Figure S3 (b) shows that the Co^{4+} transferred to Co^{3+} could be originated from spin-state transition scenario of Co ions.

Figure S4 shows temperature dependence of thermal diffusivity coefficient and specific heat for the composites. It can be seen that the λ values decreased gradually with the increasing of measured temperature. And the C_p of the composites reached 0.66 J/(g·K) at 1073 K for the x=0.09 sample.

Figure S5 shows the Raman vibration of composites at room temperature. The vibration of

heavier Ca or Co atoms occurred in the low wavenumber, while the vibration of light O atom occurred in the high wavenumber. It could be seen that the characteristic peak of P1 represented the vibration peak of Ca atom and P2~P7 represented the vibration peak of O atom [S4, S5]. The peak at 466.3 cm^{-1} was identified as the A_{1g} mode, the peak at 615.4 cm^{-1} was the E_{1g} mode. The A_{1g} mode was associated with a Co-O stretching vibration, while the E_{1g} mode was associated with a planar O-O vibration mode.

References

[S1] Yang, W. C.; Zhang, H. C.; Tao, J. Q.; Zhang, D. D.; Zhang, D. W.; Wang, Z. H.; Tang, G.D. Optimization of The Spin Entropy by Incorporating Magnetic Ion in A Misfit-Layered Calcium Cobaltite. Ceram. Int. 2016, 42, 9744-9748.

[S2] Noudem, J. G.; Kenfaui, D.; Chateigner, D.; Gomina, M. Toward The Enhancement of Thermoelectric Properties of Lamellar $Ca_3Co_4O_9$ by Edge-free Spark Plasma Texturing. Scripta Mater. 2012, 66, 258-260.

[S3] Butt, S.; Xu, W.; He, W. Q.; Tan, Q.; Ren, G. K.; Lin, Y. L.; Nan, C. W. Enhancement of Thermoelectric Performance in Cd-doped $Ca_3Co_4O_9$ Via Spin Entropy, Defect Chemistry and Phonon Scattering. J. Mater. Chem. A 2014, 2, 19479-19487.

[S4] Lemmens, P.; Choi, K. Y.; Gnezdilov, V.; Sherman, E. Y.; Chen, D. P.; Lin, C. T.; Chou, F. C.; Keimer, B. Anomalous Electronic Raman Scattering in $Na_xCoO_2{\cdot}yH_2O$. Phys. Rev. B 2006, 96, 16720401-16720404.

[S5] Hong, W. T.; Gadre, M.; Lee, Y. L.; Biegalski, M. D.; Christen, H. M.; Morgan, D.; Horn, Y. S. Tuning The Spin State in $LaCoO_3$ Thin Films for Enhanced High-temperature Oxygen Electrocatalysis. J. Phys. Chem. Lett. 2013, 4, 2493-2499.

List of Table in Supporting Information

Table S1 Concentration of different elements for the XPS fitting results.

x	Sliver/%		Cobalt/%		Oxygen/%		
	Ag^{+}	metallic Ag	Co^{3+}	Co^{4+}	O_{abs}	V_O	O_{lat}
0.03	92.5	7.5	39.7	60.3	25.8	16.2	58.0
0.06	90.1	9.9	40.8	59.2	30.2	19.3	50.5
0.09	88.0	12.0	43.7	56.3	30.6	15.4	54.0
0.12	86.1	13.9	44.6	55.4	35.3	18.2	46.5

List of Figures in Supporting Information

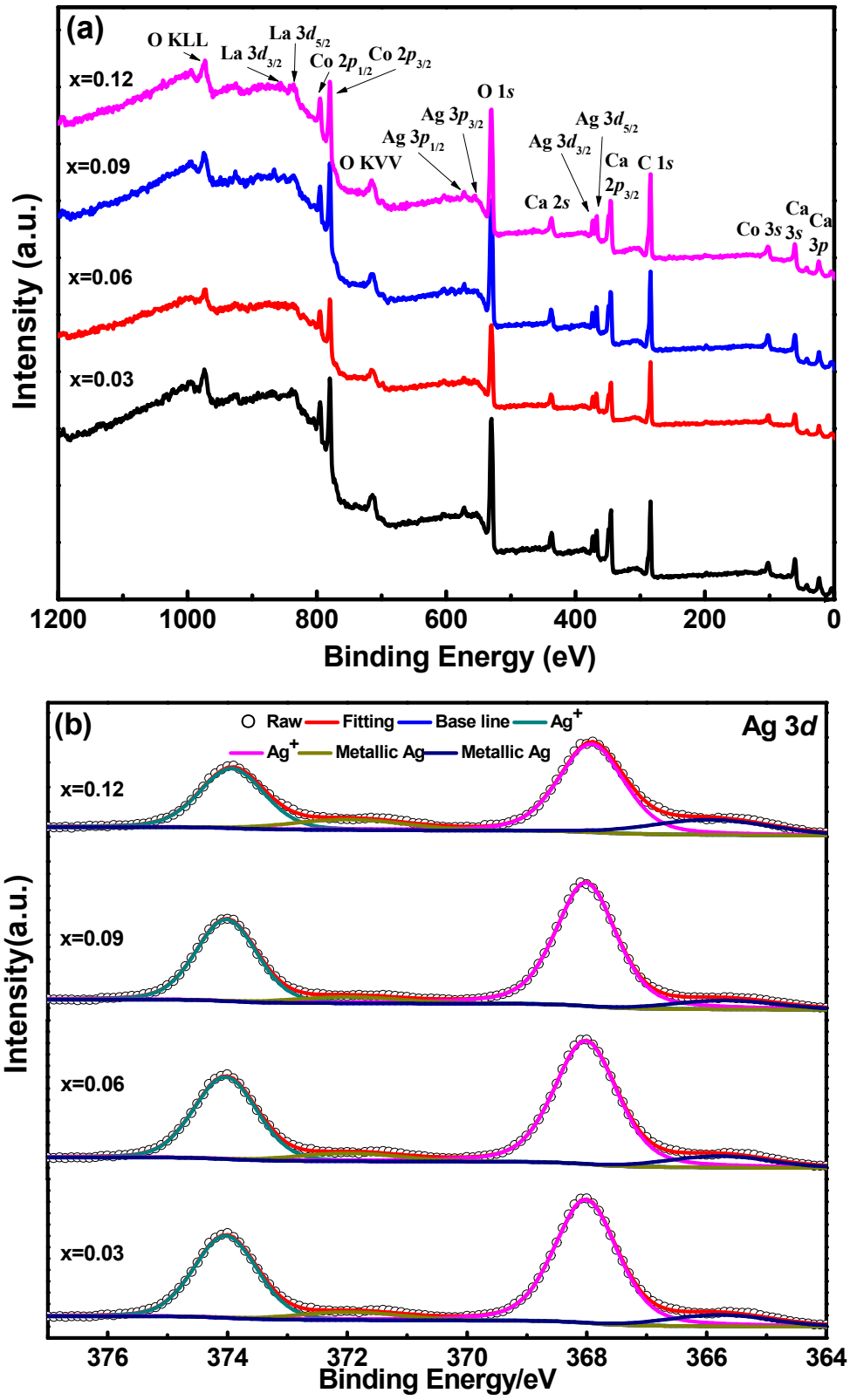

Figure S1 XPS survey spectra for composites. (a) full XPS survey spectra, (b) high-resolution of Ag 3*d*

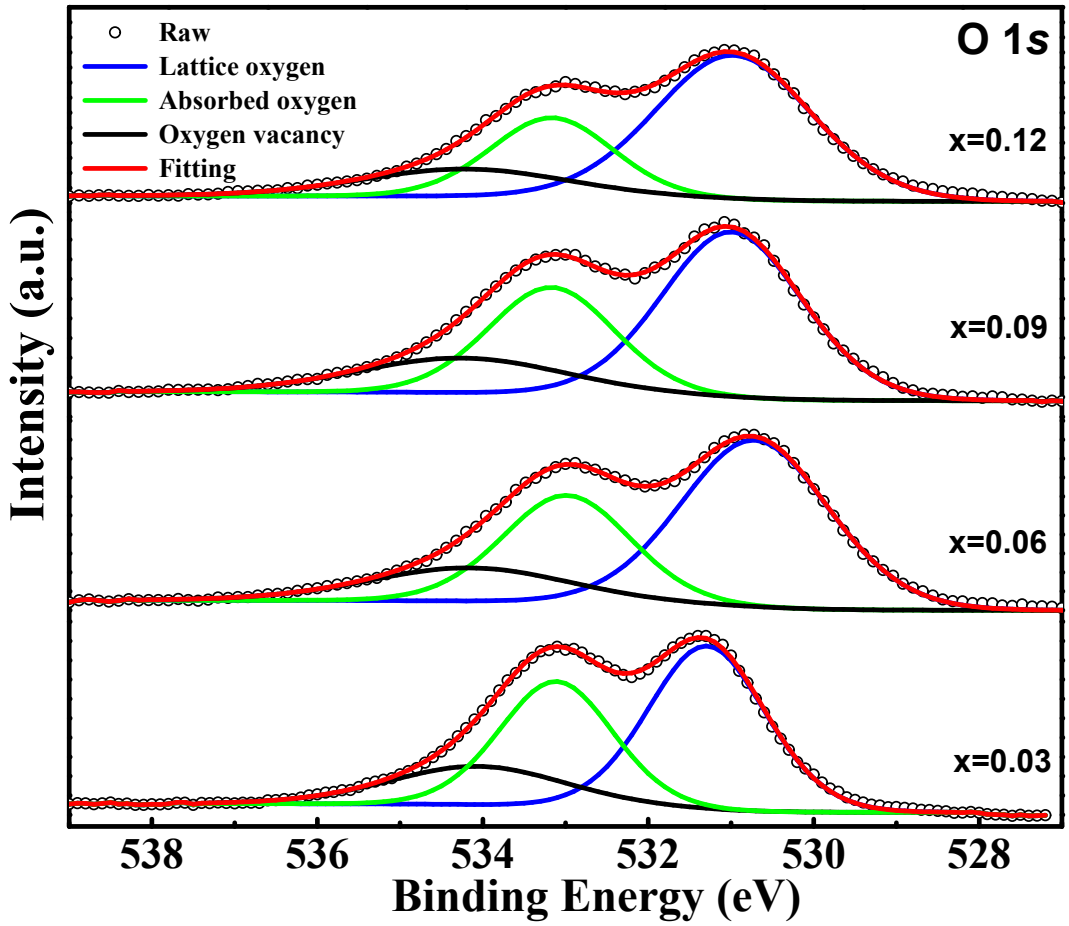

Figure S2 High-resolution XPS spectra for O 1*s*.

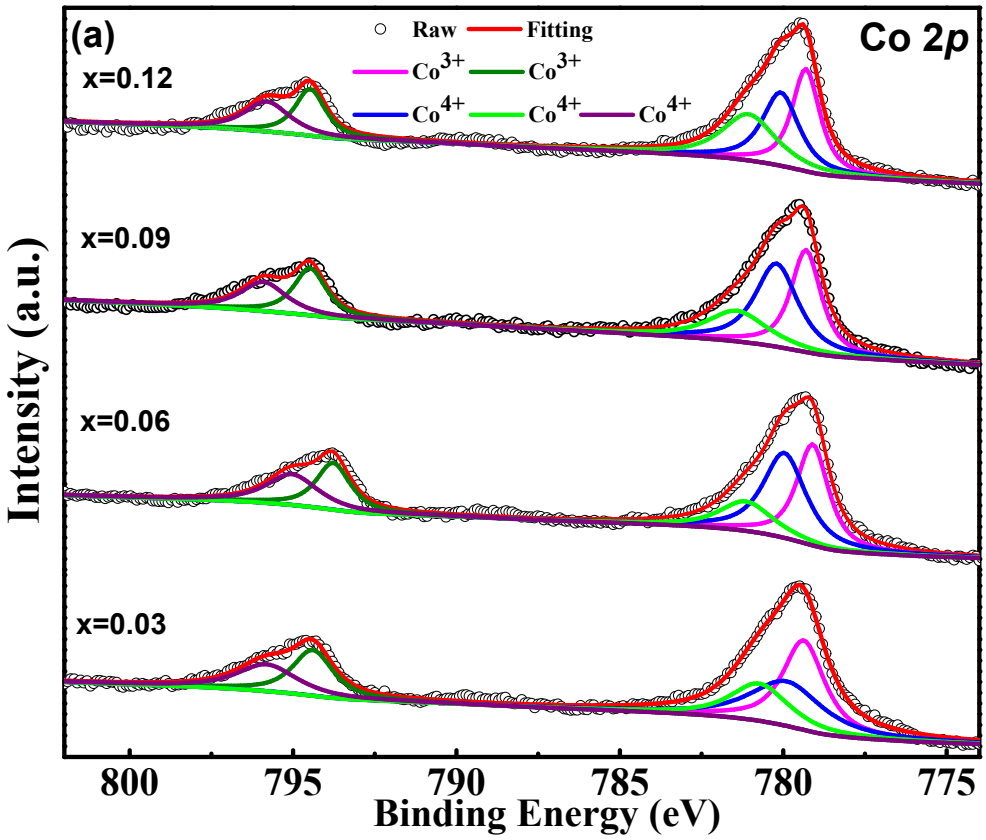

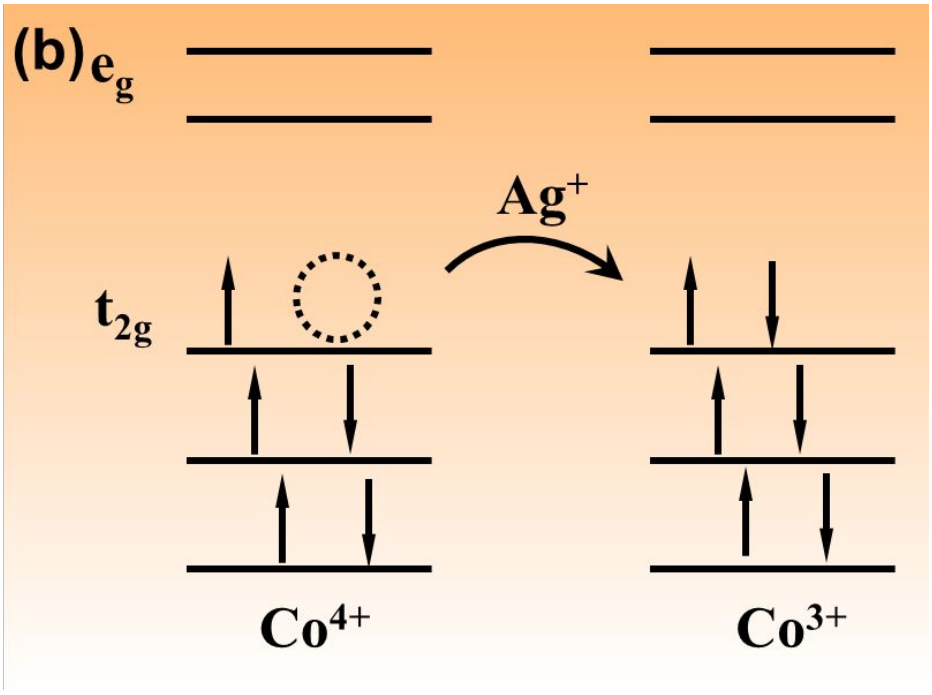

Figure S3 (a) High-resolution XPS spectra for Co 2*p*, (b) spin-state transition scenario.

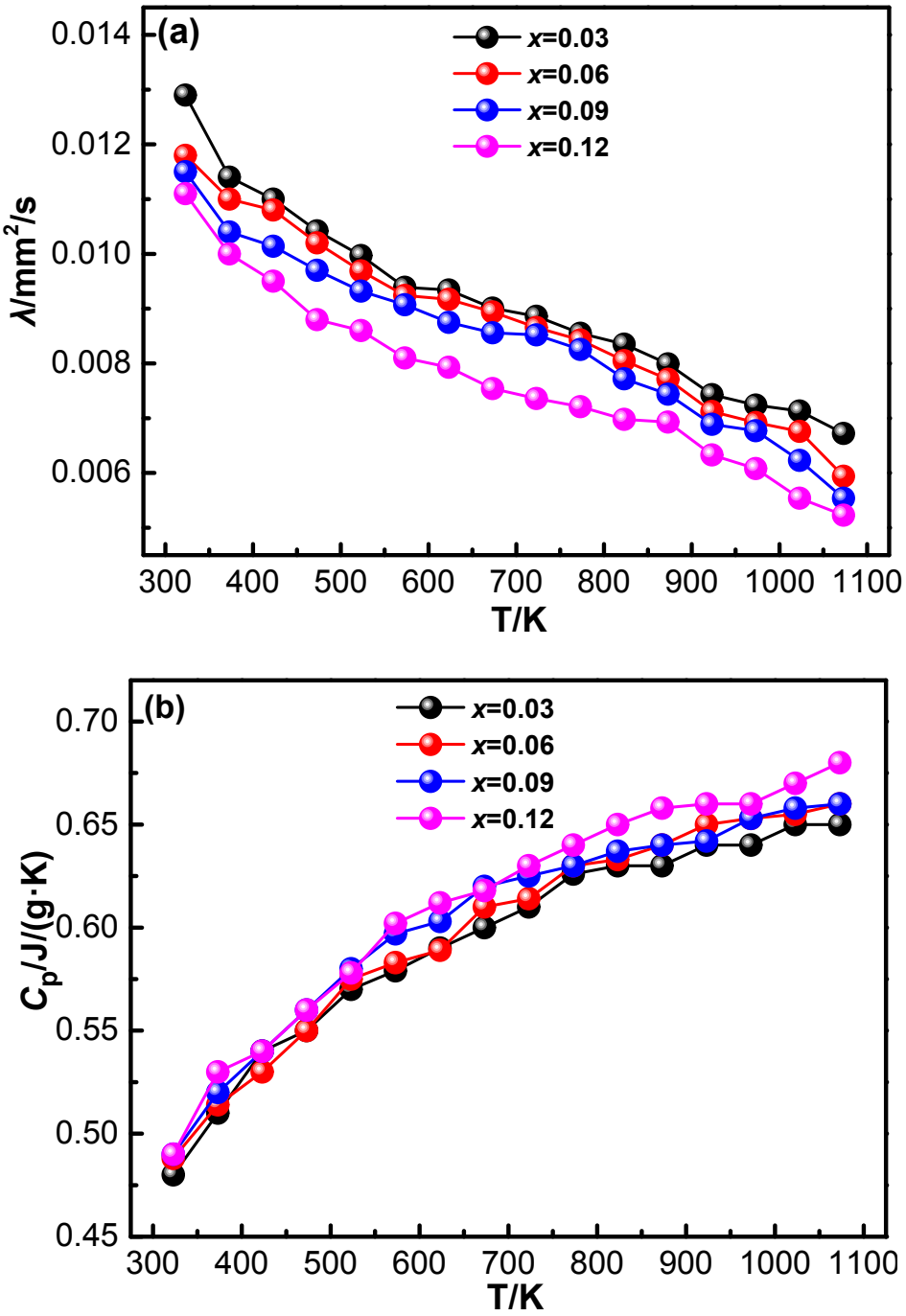

Figure S4 Temperature dependence of thermal diffusivity coefficient and specific heat for the composites. (a) thermal diffusivity coefficient, (b) specific heat

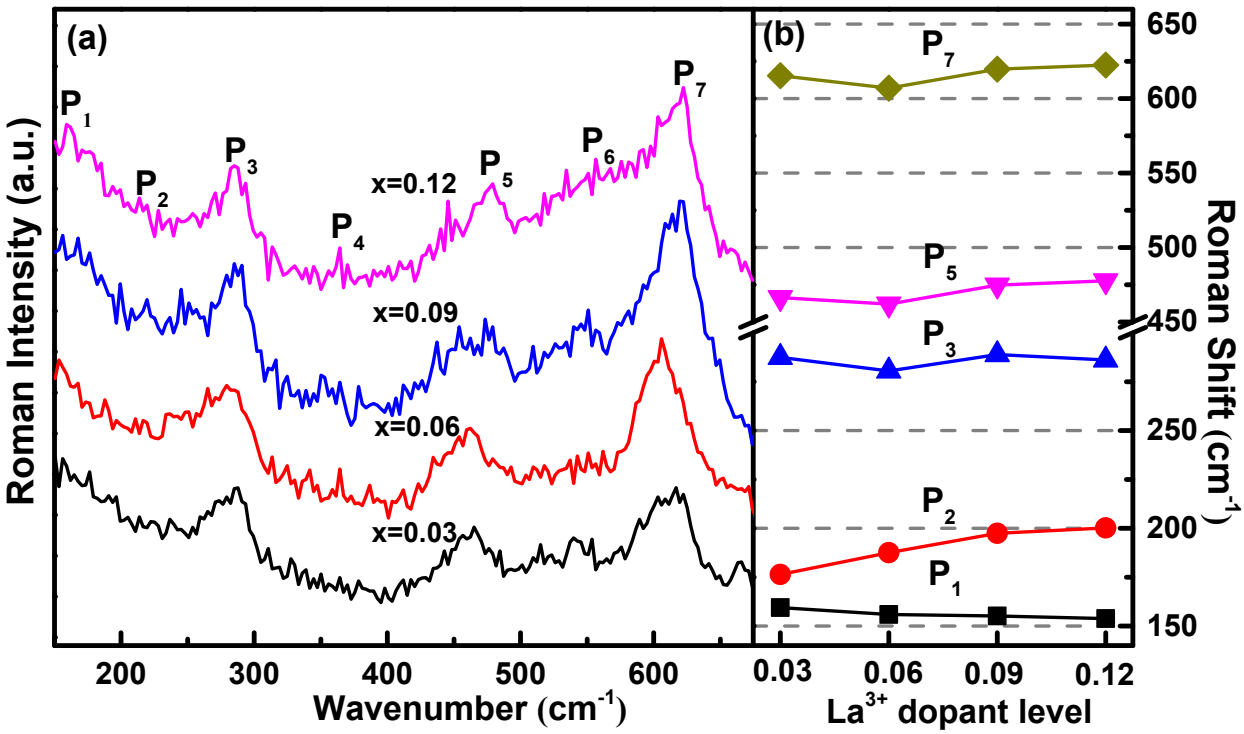

Figure S5 (a) Raman spectra for composites (b) Raman wave numbers P_1, P_2, P_3, P_5, and P_7